Energy 46 (2012) 555–563

Contents lists available at SciVerse ScienceDirect

Energy

journal homepage: www.elsevier.com/locate/energy

An assessment of wind energy potential at the demonstration offshore wind farm in Korea

Ki-Yong Oh*, Ji-Young Kim, Jae-Kyung Lee, Moo-Sung Ryu, Jun-Shin Lee

Green Growth Laboratory, KEPCO Research Institute, Daejeon 305-760, Republic of Korea

ARTICLE INFO

Article history:
Received 31 January 2012
Received in revised form
16 May 2012
Accepted 28 July 2012
Available online 10 September 2012

Keywords:
Offshore wind farm
Offshore wind energy
Wind turbine
Annual Energy Production
Capacity Factor
Feasibility study

ABSTRACT

The construction of an offshore demonstration wind farm was planned in a southwestern sea-area of the Korean Peninsula. To estimate economic feasibility and to establish a reliable design basis, it is necessary to identify the design parameters of the demo-farm. For a reliable estimation of the design parameters, the first offshore meteorological mast, HeMOSU (Herald of the Meteorological and Oceanographic Special Research Unit), was constructed at the site of the demo-farm. In addition, supplementary meteorological masts were installed in advance at Gochang and Wangdeung-do in order to enhance the estimation of the long-term wind potential for the demo-farm. In this paper, assessments of wind energy potential are carried out with the data measured from these three meteorological masts. The analysis includes seasonal and diurnal changes in wind speed and surface roughness as well as wind/energy rose. Long-term wind potential is also estimated by using MCP (Measure-Correlate-Predict) techniques to clarify the design basis and to determine the wind turbine class in accordance with IEC 61400. The AEP (Annual Energy Production), as well as the C.F. (Capacity Factor) of the candidate site are evaluated with the estimated design parameters.

1. Introduction

The necessity of developing renewable energy is on the rise throughout the world because of climate change and the exhaustion of fossil fuel-based energy sources. Among renewable energies, wind energy is the fastest growing source of energy and is receiving worldwide attention due to the latest technology for harnessing its power. Utilization of wind power is the answer to environmental and climate change problems and is a means of conserving conventional sources of energy. To catalyze the development of wind farm, several in-depth research projects have been accomplished in assessments of wind potential and prediction of wind energy all over the world [1–5].

Offshore wind energy in particular provides higher energy density, has smaller restrictions of scale and is less likely to generate civil complaints than onshore wind energy. Accordingly, many countries throughout the world have been making efforts to exploit offshore wind energy.

Mountainous regions cover 70% of Korean territory and the numbers and sizes of arable plains suitable for wind energy are negligibly small. Reflecting these geomorphologic characteristics, the development of offshore wind farms on the Korean Peninsula is widely perceived as being essential to fulfilling the national target for renewable energy.

Evaluation of wind variation and wind potential by season and diurnally is conducted in order to investigate the feasibility of offshore wind power off the coast near Jeju-do, famed for having the best wind resources in Korea [6,7]. Jang et al. [8] assessed offshore wind resources around the Korean Peninsula through analyses of long-term QuikSCAT data; Kim et al. [9,10] developed a high precision numerical wind map for coastal areas of the Korean Peninsula in order to ensure a systematic survey of the feasibility of offshore wind power. The results of these studies only refer to wind energy resources, even though any feasibility study of offshore wind farms should address estimation of design parameters, clarification of wind turbine class, and prediction of energy production.

This paper presents our overall analyses in order to allow for the design of offshore wind farms and to accomplish a feasibility study of a demo-farm. First of all, wind resource assessment is conducted to identify design parameters such as wind potential, vertical wind profile, and air density. In addition, wind turbine class for the demo-farm is clarified through an analysis of extreme wind speed and turbulence intensity, in accordance with IEC 61400. To enhance the reliability of the analysis, the MCP (Measure-Correlate-Predict) technique is introduced in the evaluation of the wind turbine class. To allow for a secure feasibility study, AEP (Annual Energy

* Corresponding author. Tel.: +82 42 865 5376; fax: +82 42 865 7659.
E-mail addresses: okyer@kepco.co.kr, okyer@kepri.re.kr (K.-Y. Oh).

0360-5442/$ – see front matter
http://dx.doi.org/10.1016/j.energy.2012.07.056

Production) and C.F. (Capacity Factor) are, finally, evaluated with site-specific parameters.

2. Geographical location and measurement stations

It was suggested that we locate the demo-farm in the southwestern sea-area of the Korean Peninsula due to crucial factors of economic feasibility, including wind potential, sea depth, and distance from existing substations and their capacity [11]. For reliable estimation of the economic feasibility and the establishment of the design basis of the demo-farm, an offshore meteorological mast was installed in October 2010, as shown in Fig. 1.

In order to measure the wind potential at the hub level of a 3–7 MW class offshore wind turbine, anemometers were installed at heights of 76 m, 86 m, 96 m, and 97 m with respect to the mean sea level; wind vanes were installed at heights of 76 m and 96 m. To investigate the vertical wind profile of the offshore winds, anemometers and wind vanes were also installed at heights of 26 m, 46 m, 56 m, and 66 m. Temperature/humidity sensors and barometers were installed at heights of 13 m and 94 m in order to calculate the air density necessary for Annual Energy Production of the wind farms. The details of the sensor installation types and heights are shown in Fig. 2(a); specifications are shown in Table 1.

Before erecting the HeMOSU (Herald of the Meteorological and Oceanographic Special Research Unit), auxiliary meteorological masts were installed at Gochang and Wangdeung-do to consider main wind directions. A meteorological mast was installed at the Gochang Power Testing Center and erected in November 2008. The details of the configuration are shown in Fig. 2(b).

Because of wind speed reductions from increasing surface roughness on land, another supplementary meteorological mast was erected at Wangdeung-do in September 2009. Because Wangdeung-do is about 20 km northwest of Wi-do and there are no obstacles to the main wind direction, prediction of the wind potentials on this site can be compensated for correctly with measured data from Wangdeung-do. Wangdeung-do is an optimal location, but it is a difficult site for the installation of a meteorological mast because of its narrow area and steep slope. Therefore, as shown in Fig. 1, measurement equipment was installed at an unmanned telecommunications tower located at the top of the mountain (altitude of 184 m). The height of the mobile telecommunications tower is approximately 8 m but the tower has multiple pieces of telecommunications equipment and devices; therefore, it is likely to disturb wind speed. To minimize wake disturbances from other devices, the height of measurement is 12 m, with an extended boom. Two anemometers, one wind vane, a thermo/humidity sensor, and a barometer were installed to the northwest, which is the main wind direction.

Fig. 1. Geographical positions of meteorological mast.

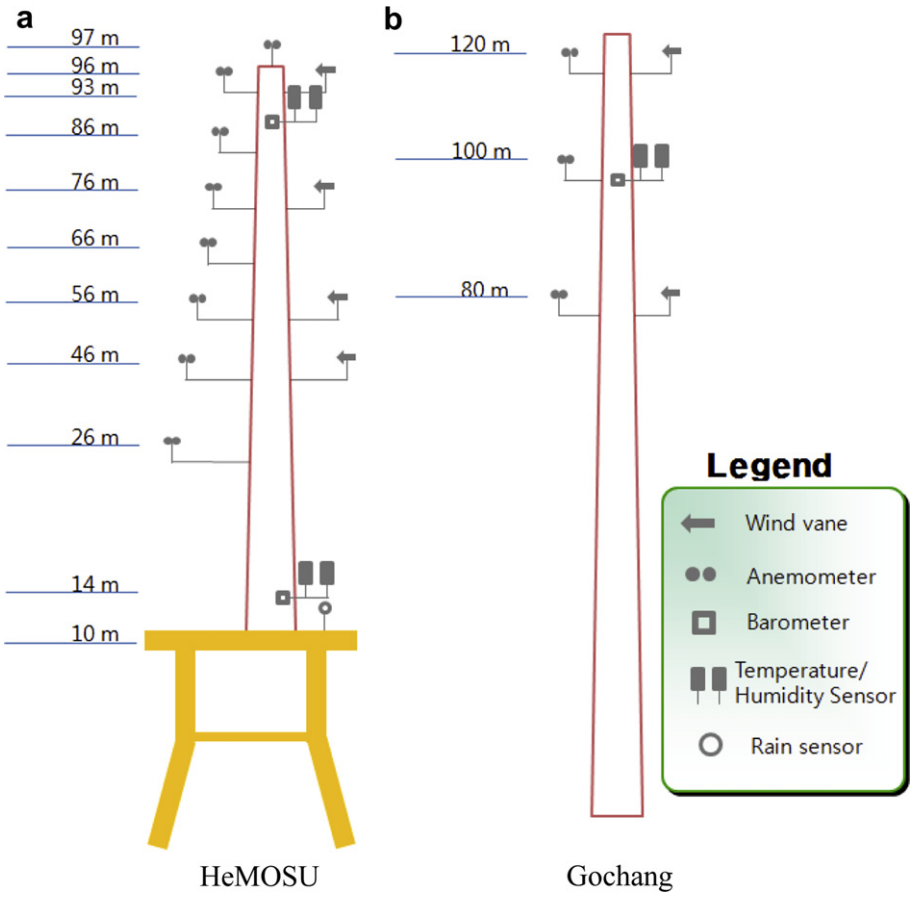

Fig. 2. Sensor type and installation height.

Geographical location and measurement periods are shown in Table 2.

3. Assessments

3.1. Wind potential

The data validation has been accomplished. The wind data has been subjected to a quality check procedure to identify records affected by equipment malfunctions and other anomalies. The recovery rate of data for the complete set of measurement periods at each meteorological mast is 90.8%, 99.8%, and 98.8%, which is considered reasonable for reliable analysis.

Table 1
Main technical parameters of sensors.

	Anemometer	Wind vane	Barometer	Thermo/humidity sensor
Measurement range	0–75 m/s	0–360°	800–1100 hPa	−30–70 °C
Resolution	0.1 m/s	0.1°	1 hPa	0.1 K
Accuracy	0.1 m/s (0.1–10 m/s) 1% (10–55 m/s) 2% (55–75 m/s)	±4° In steady winds over 3 m/s	±1%	±0.2 K
Starting threshold	0.15 m/s	1°	N/A	N/A
Operation temperature	−55–55 °C	−30–70 °C	−40–85 °C	−30–80 °C

Fig. 3 illustrates the monthly average wind speed from the data measured at HeMOSU, Wangdeung-do, and Gochang using Eq. (1) [3]. The data measured at HeMOSU describes only wind speeds at heights over 80 m, a hub height of multi-MW class wind turbines used for offshore wind farms.

$$V_{\text{ave}} = c\Gamma\left(1+\frac{1}{k}\right), \tag{1}$$

where V_{ave}, Γ, c and k represent average wind speed, gamma function, scale factor, and shape factor, respectively.

According to the actual measurement data of HeMOSU, as shown in Fig. 3, the data measured from June to July shows a large range of fluctuations compared to the data measured by the auxiliary meteorological masts. The reason is that an approximately 50% data loss occurred during June and July. To identify the problem, an analysis of the voltage levels in the data acquisition system was conducted. In this analysis, it was found that the data logger frequently turned off during long spells of rainy weather and when a typhoon passed through the met-mast. The power supply system was composed of two small wind power generators and assorted solar power generators. When a typhoon passed through the site, one small wind power generator was broken. In addition, the photovoltaic system could not sufficiently generate power due to lack of sunlight. For reliable power supplies, necessary to prevent recurrence of these problems, the photovoltaic system has been strengthened and the supplied power voltage is being monitored in real-time. Since this strengthening of the power systems, power problems and data loss have not occurred.

Table 2
Specific information of met-mast.

Site	Latitude	Longitude	Measurement period	Average interval
HeMOSU	N35°27′55.16″	E126°07′45.30″	2010.10.18–2011.10.19	10 m
Wangdeung-do	N35°39′43.27″	E126°06′23.66″	2009.09.23–2011.10.13	10 m
Gochang	N35°27′42.78″	E126°26′58.95″	2008.11.21–2011.09.26	10 m

One year's worth of data from HeMOSU revealed average wind speeds, showing delicate differences according to height measured in the range of 6.7–6.9 m/s. Wind energy density is 383.5 W/m^2, 395.7 W/m^2, and 418 W/m^2 at 86 m, 96 m and 97 m, respectively. The energy density was calculated using Eq. (2) [3].

$$P = \int_0^\infty \frac{1}{2}\rho v^3 f(v)\,\mathrm{d}v = \frac{1}{2}\rho c^3 \Gamma\left(\frac{k+3}{k}\right), \tag{2}$$

where P, ρ, v, and $f(v)$ represent energy density, air density, wind speed, and the probability density function of the Weibull distribution, respectively.

Fig. 4 shows the Weibull distribution of HeMOSU used to calculate the energy density. It can be seen that the scale factor (c) is 7.5–7.8 and the shape factor (k) is approximately 1.8, which is smaller than the normal value. Table 3 presents comparisons between measured wind potential and that shown on the KIER wind map [12]. Comparisons were accomplished using data from the 86 m height because the height of the wind map is 80 m. Error is less than 5%, which is considered to be reasonable. Measured data is similar to that of the numerical wind map, although the measurements are only for one year; the numerical wind map contained 10 years of data. The smaller the shape factor, the wider the distribution. This means that energy production is increased at the same mean wind speed. The site for the demo-farm is appropriate for wind generation.

Significant seasonal wind variations exist, including the monsoon influence on the Korean peninsula. Wind speed may not correspond precisely with wind energy density [12]. As wind energy is proportional to the cube of wind speed, even for the same mean wind speed, the large seasonal differences cause a mismatch of wind classifications between wind speed and wind energy density. Since wind speed in wind classifications is converted from energy density, assuming wind density is a Rayleigh probability distribution with a 1/7 wind shear exponent, systematic study of demo-farms was conducted according to the energy density. Even

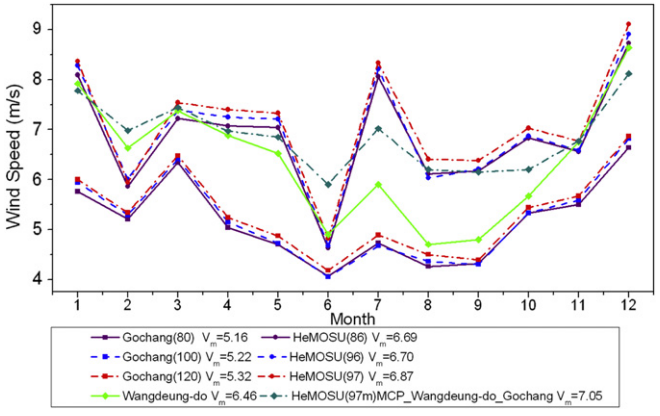

Fig. 3. Monthly wind speed (m/s).

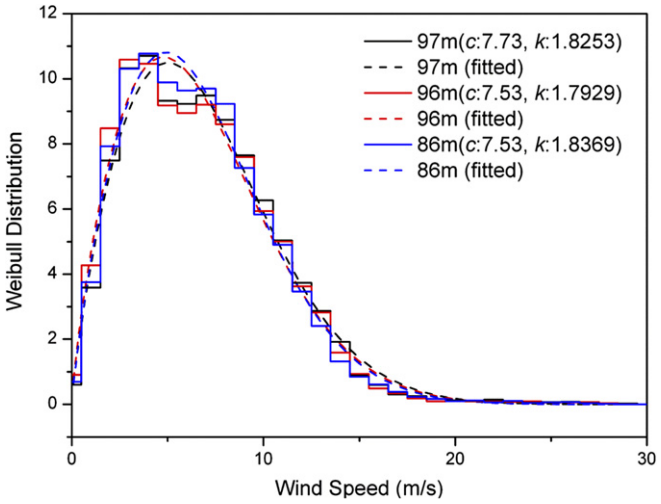

Fig. 4. Weibull distribution.

though Wind Class 3 is observed at a height of 80 m, Wind Class 2 is observed at a height of 100 m, as shown in Table 4 [13]. As HeMOSU is installed in the sea, roughness is relatively smaller than onshore and the wind class seems to differ according to height alone. Optimum height needs to be estimated in the wind farm design because the change of wind class by height is relatively small.

Despite being close to the coast, data from the Gochang met-mast shows a low average wind speed compared to those at HeMOSU and Wangdeung-do. Considering that Gochang's meteorological mast is 21 km away from Wi-do, its low wind speed may be caused by geomorphologic influences rather than the wake effect of the island. Jang and Ryu et al. [14] analyzed the wake effect by carrying out a CFD simulation with the model of Wi-do. From these analyses, wake loss of about 5% was measured in this area at 15 km distance. Accordingly, to consider economic feasibility, offshore wind farms should be constructed away from coasts to prevent wind energy loss from geomorphologic influences.

The design lifespan of a wind turbine is 20 years. Therefore, the economic efficiency of an offshore wind farm should be evaluated every 20 years. A long-term analysis of wind resources should be carried out using data from surrounding areas with the introduction of the MCP technique [15] because data measured at HeMOSU were taken over a period of one year. In this study, long-term wind resources at the demo-farm were predicted by using data measured at the auxiliary meteorological masts at Wangdeung-do and Gochang. It was observed that the coefficient of determination (R^2) with the Wangdeung-do data is 0.97, higher than that with the Gochang data (0.94), even though the measurement period of Wangdeung-do was shorter than that of Gochang. To secure high reliability in the assessment of the long-term wind potential, the complementary MPC technique is introduced [16]. As a result, three years' worth of data was recovered, as shown in Fig. 3. The average wind speed was 7.05 m/s; the energy density was 446.2 W/m^2. It can be observed that the long-term wind potential

Table 3
Comparison between measure data and KIER wind map.

Site	Energy density	Scale factor (c)	Shape factor (k)
HeMOSU (86 m)	385	7.53	1.84
KIER Wind map (80 m)	384	7.68	1.93
Error	0.2%	1.9%	4.6%

Table 4
Wind classification.

Wind class	10 m		50 m		80 m		100 m		120 m	
	Density (W/m^2)	Speed (m/s)	Density (W/m^2)	Speed (m/s)	Density (W/m^2)	Speed (m/s)	Density (W/m^2)	Speed (m/s)	Density (W/m^2)	Speed (m/s)
1	<100	<4.4	<200	<5.6	<240	<5.9	<260	<6.1	<290	<6.3
2	100/150	4.4/5.1	200/300	5.6/6.4	240/380	5.9/6.9	260/420	6.1/7.1	290/450	6.3/7.3
3	150/200	5.1/5.6	300/400	6.4/7.0	380/490	6.9/7.5	420/560	7.1/7.8	450/600	7.3/8.0
4	200/250	5.6/6.0	400/500	7.0/7.5	490/620	7.5/8.1	560/670	7.8/8.3	600/740	8.0/8.6
5	250/300	6.0/6.4	500/600	7.5/8.0	620/740	8.1/8.6	670/820	8.3/8.9	740/880	8.6/9.1
6	300/400	6.4/7.0	600/800/	8.0/8.8.	740/970	8.6/9.4	820/1060	8.9/9.7	880/1160	9.1/10.0
7	>400	>7.0	>800	>8.8	>970	>9.4	>1060	>9.7	>1160	>10.0

at a height of 97 m was greater than the value found in the actual measurement data. The presumption is that the wind in the measured year was not as consistent as it was in other years. The site for the demo-farm is suitable because it meets minimum Wind Class 3 at all heights, considering long-term wind potential.

Fig. 5 illustrates the average diurnal variations in wind speed. According to the measurement data of the Gochang met-mast, wind speed increases at 10 AM, to reach its maximum value at 2 PM. Wind speed decreases thereafter and the maximum difference is approximately 1.418 m/s. The wind speed at HeMOSU increases at 1 PM, reaching a maximum value at 5 PM. Its maximum variation is 1.125 m/s. The wind speed measured on the Wangdeung-do meteorological mast decreases at 6 AM and reaches its minimum value at 11 AM. The wind speed increases again, resulting in a difference of 1.377 m/s. By observing the measurement data for the three meteorological masts, it can be seen that constant wind begins at daybreak, but that wind speed varies during the daytime because of temperature changes. Wind speed variation on land is faster than it is offshore. This is because the earth's surface is quickly heated by solar heat. This difference in specific heat works as a factor in creating wind speed variations that are greater onshore than offshore, so the maximum daily wind speed variation at Gochang (1.418 m/s) is relatively large compared to that of HeMOSU, which is located at sea (1.125 m/s).

Fig. 6 illustrates the wind rose and energy rose, measured from HeMOSU. The frequencies for the three main wind directions, NNW/N/S, are 18.01%, 13.46%, and 12.83%, respectively. The energy rose is superior in the direction of S/NNW/SSE, as illustrated in Fig. 6(b), because high quality wind, over the rated wind speed, rises mostly in these directions. This phenomenon occurred because a typhoon passed from south to north in the summer season of the measured year. In the design of the farm layout, meteorological characteristics such as typhoons and the monsoon should be taken into consideration.

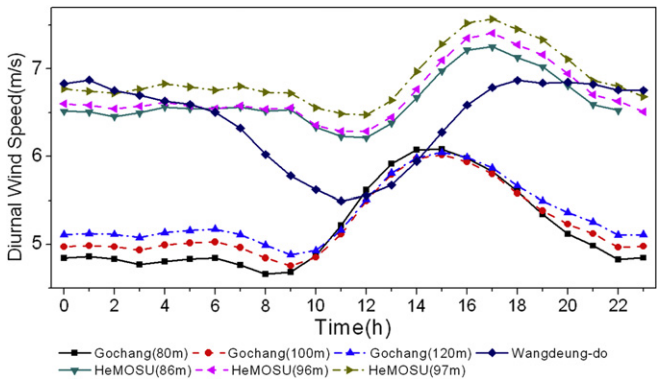

Fig. 5. Diurnal wind speed (m/s).

3.2. Vertical wind profile

A survey of surface roughness should be made in order to determine the optimal hub height of offshore wind turbines for maximization of economic feasibility because wind speed varies by height depending upon surface roughness. In this study, anemometers were installed at eight different heights in HeMOSU in order to estimate a highly reliable roughness for the demo-farm. The power law profile was used for the investigation of the vertical wind profile, as shown in Eq. (3)

$$V_{\mathrm{h}} = V_{h_{\mathrm{r}}}\left(\frac{h}{h_{\mathrm{r}}}\right)^{\alpha}, \tag{3}$$

where V denotes wind speed and α is the wind shear exponent. Subscripts h and h_{r} are measured height and reference height, respectively. Estimation of the wind shear exponent is accomplished with 8 sets of height data by using regression analysis.

It can be seen in Fig. 7 that the average power law exponent is 0.130, smaller than the value 1/7 used for onshore sites. However, this value of 0.130 is larger than the values 0.11 or 0.12, which were suggested for offshore in previous studies [17,18]. Because the west coast is a gulf, surrounded by the Korean peninsula and the eastern part of China, the site for the demo-farm is substantially affected by geomorphologic influences. Ocean areas without nearby obstacles are less affected. Therefore, it is considered that surface roughness here is slightly larger. Fig. 7(a) illustrates the variation of the wind shear exponent by average day/night. It can be observed that the wind shear exponent in the daytime is slightly smaller than that at night. This phenomenon is normally caused by atmospheric instability due to temperature changes with altitude [19]. It can be deduced by looking at this phenomenon that wind shear will cause greater fatigue load during the nighttime because the surface roughness during the daylight hours is lower than it is at night. Fig. 7(b) illustrates the seasonal variations of surface roughness. The surface roughness during the fall and winter is relatively small even though the offshore roughness increases to the same level as that of the land roughness during the spring and summer. It seems that surface roughness is high during the summer because the Korean Peninsula has relatively unstable weather conditions due to the rainy season and frequency of typhoons. Seasonal variations of wind speed can also be observed in this graph. The graph shows that the average wind speed in summer is relatively low while that in winter is at its highest. The graph also shows that the spring is better than fall. Periodic maintenance of offshore wind farms will be optimally planned for summer months. Summer power production is relatively small in consideration of wind speed variations by season.

3.3. Air density

Air density should also be investigated during feasibility surveys of wind development because wind energy is proportional to air

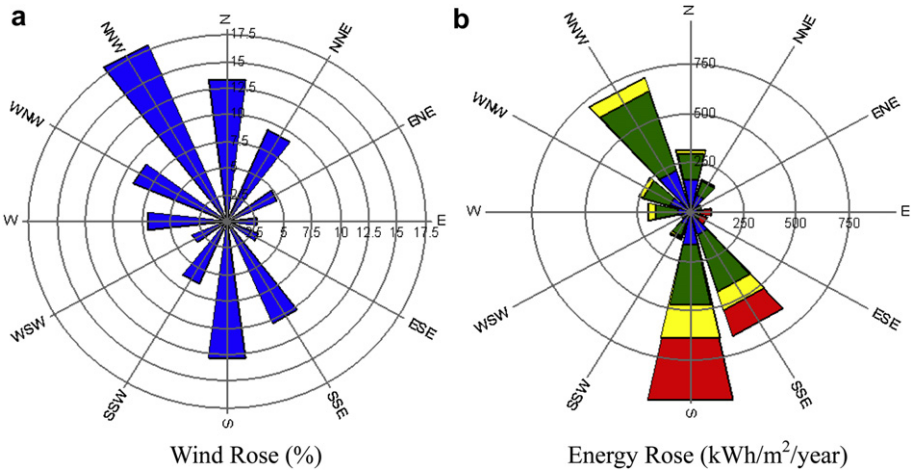

Fig. 6. Wind/energy rose (m/s).

density. In this paper, air density was calculated according to Eq. (4) by installing a barometer and a temperature sensor at heights of 14 m and 93 m on HeMOSU for purposes of measuring air density on the surface and at the hub height [20].

$$\rho_{10\ \mathrm{min}} = \frac{B_{10\ \mathrm{min}}}{R_0 T_{10\ \mathrm{min}}}, \tag{4}$$

where $\rho_{10\ \mathrm{min}}$ is the derived 10 min averaged air density, $T_{10\ \mathrm{min}}$ is the measured absolute air temperature averaged over 10 min, $B_{10\ \mathrm{min}}$ is the measured air pressure averaged over 10 min, and R_0 is the gas constant of dry air, 287.05 J/(kg K).

Fig. 8 illustrates the calculated air density histogram. Red (in the web version) is the histogram of air density calculated at 13 m; blue (in the web version) is the histogram of air density calculated at 94 m. You will notice that air density is uniformly distributed in range of 1.24–1.30. The average air density values measured at 13 m and 94 m are 1.268 kg/m^3 and 1.252 kg/m^3 respectively. These values of measured air density are 3.5% and 2.2%, respectively, higher than 1.225 kg/m^3, the standard air density. Compared to that of other areas, energy production at the demonstration wind farm is expected to increase even when the same wind turbine is applied to all areas.

Considering the wind shear exponent and air density, lowering the hub height of the wind turbines at the demo-farm candidate site is considered advantageous because it can reduce construction costs and increase Annual Energy Production.

4. Clarification of wind turbine class at demo-farm

4.1. Extreme wind speed

IEC suggests that wind turbine classes be created to include extreme wind speeds (EWS) and turbulence intensity [21,22]. Extreme wind speeds are classified into three types, I/II/III in IEC 61400-1. Each reference extreme wind speed, V_{ref}, at each class is also proposed in IEC 61400-1. V_{ref} is the extreme 10 min average wind speed with a recurrence period of 50 years at turbine hub height. Manufacturers design wind turbines to endure the aerodynamic load that corresponds to the reference extreme wind speed with a recurrence period of 50 years and with a recurrence period of 1 year at the hub height. Because each manufacturer's turbines has a different hub height, the turbine must be designed to withstand the appropriate aerodynamic load by calculating the extreme wind speed with a recurrence period of 1 year and with

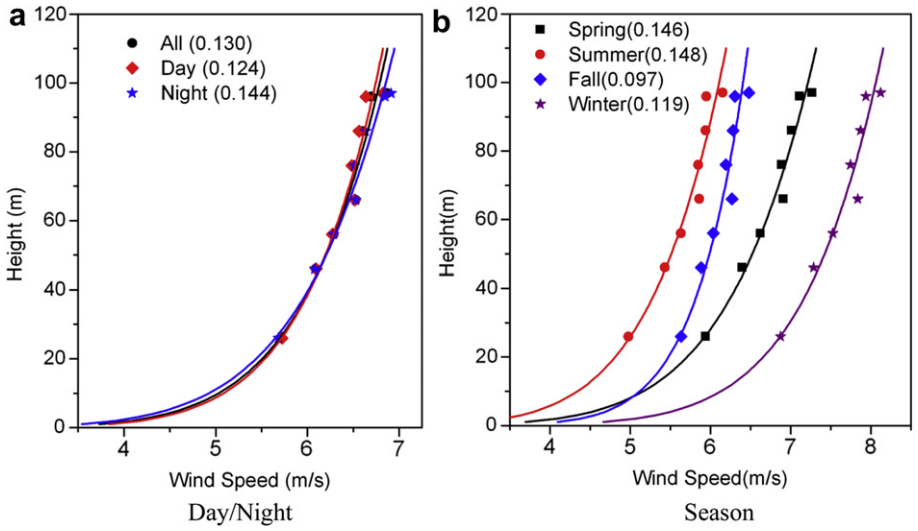

Fig. 7. Variation of the wind shear exponent.

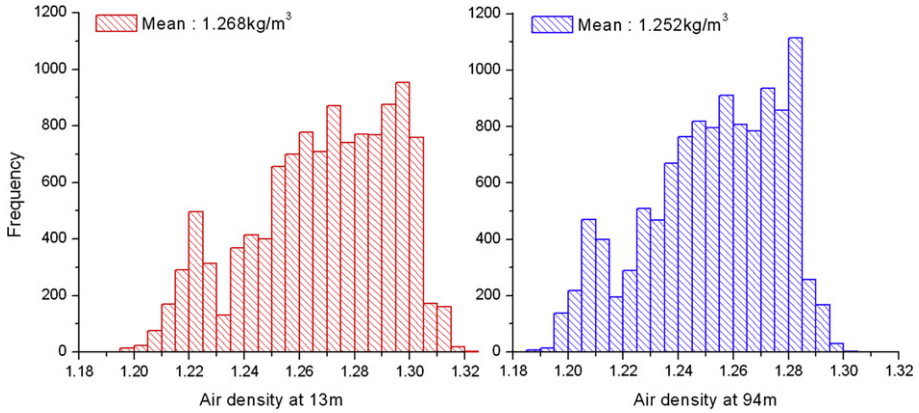

Fig. 8. Histogram of air density.

a recurrence period of 50 years, corresponding to each class and hub height, by using Eqs. (5) and (6).

$$V_{e50}(z) = 1.4V_{ref}(z/z_{hub})^{0.11}, \quad (5)$$

$$V_{e1}(z) = 0.8V_{e50}(z), \quad (6)$$

where V_e is the extreme wind speed of the 3 s average, V_{e50} is the steady extreme wind speed with a recurrence period of 50 years, V_{e1} is the extreme wind speed with a recurrence period of 1 year, and z_{hub} is the hub height.

When extreme wind speed is estimated using long-term measured data, the uncertainty of the estimation of extreme wind speed can decrease. Long-term wind data should be restored by using the complementary MCP technique based on data measured from three met-masts; then, the extreme wind speeds are calculated using the Gumbel distribution [23], as shown in Fig. 9. Table 5 shows the calculated P50 extreme wind speeds of

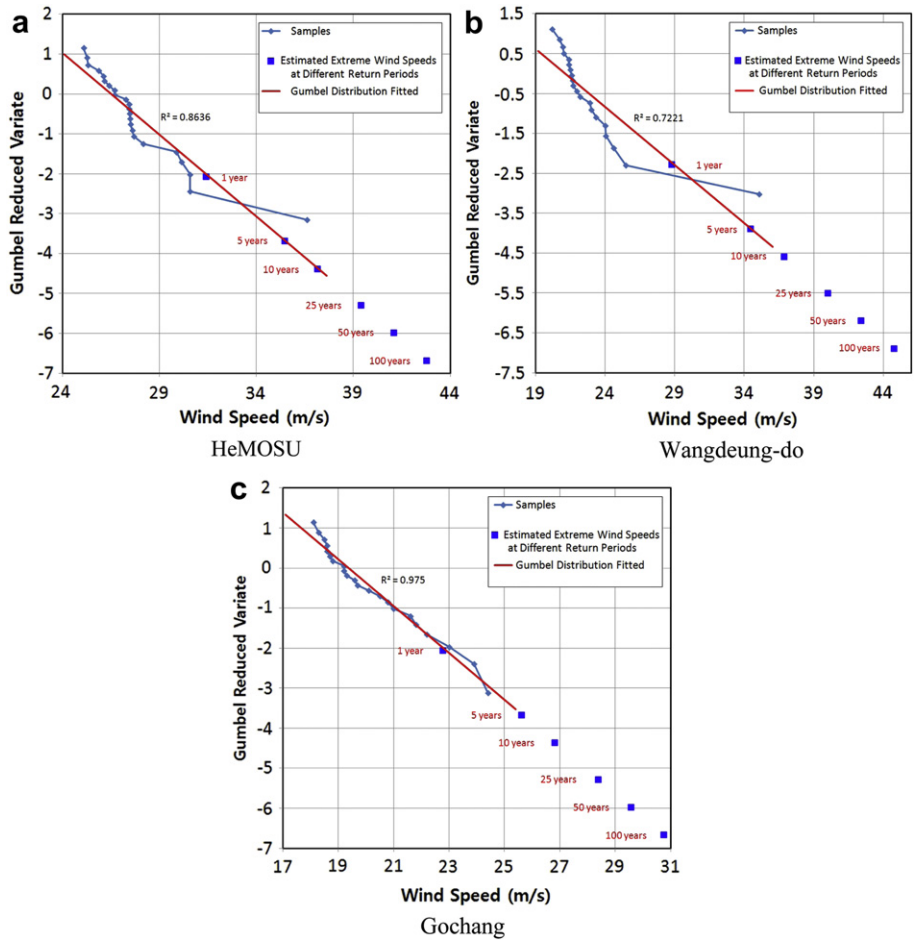

Fig. 9. Estimation of EWS with Gumbel distribution fitted.

Table 5
P50 extreme wind speed.

Return period(s)	Extreme wind speed (m/s)		Turbine class
	1 Year	50 Year	
HeMOSU (97 m)	31.6	41.1	II
Gochang (120 m)	22.9	29.6	III
Wangdeung-do	29.0	42.4	II

HeMOSU and the supplementary meteorological masts. The EWS of Gochang is very low in that it seems to have infrequent wind gusts and low average wind speed. However, the ESW of Wangdeung-do and HeMOSU is high because of frequent high-speed winds. Installing turbines of at least II and higher at the demo-farm seems to be a safe choice. Given the prevalence of typhoons, higher-class turbines are recommended for the offshore Korean peninsula.

4.2. Turbulence intensity

The second criterion is turbulence intensity, which can be classified into three classes A/B/C. Turbulence intensity is expressed by the ratio of standard deviation to the average wind speed [21,22]. Because the wind turbine is loaded cyclically, fatigue caused by aerodynamic load can seriously affect the structural integrity of the wind turbine. The turbulence intensity criterion for fatigue load is important when the turbine is designed. Fig. 10 illustrates the turbulence intensity prescribed by the IEC standard and the turbulence intensity measured from HeMOSU. In Fig. 10, the dotted line is the turbulence intensity specified by the IEC standard; the straight line is the turbulence intensity at the measured height. It is possible to use a wind turbine designed with all classes of turbulence intensity because measured turbulence intensity is extremely small. The surface roughness at HeMOSU is less than that at other areas, so the turbulence intensity at HeMOSU seems to be small. Turbulence intensity becomes relatively less of a critical factor compared to extreme wind speed during selection of the optimum turbine.

4.3. Estimation of applicable turbines and performance

Based on the results of analyzing extreme wind speed and turbulence intensity, a Class II or higher wind turbine (in terms of extreme wind speed) and C or higher (in terms of turbulence intensity) wind turbine is appropriate for the demo-farm. With an available offshore wind turbine that meets these conditions, the Annual Energy Production (AEP) and Capacity Factor (C.F.) were calculated by using Eqs. (7) and (8), in order to assess the economic feasibility of the demo-farm. Table 6 shows the calculated Annual Energy Production (AEP) and Capacity Factor (C.F.).

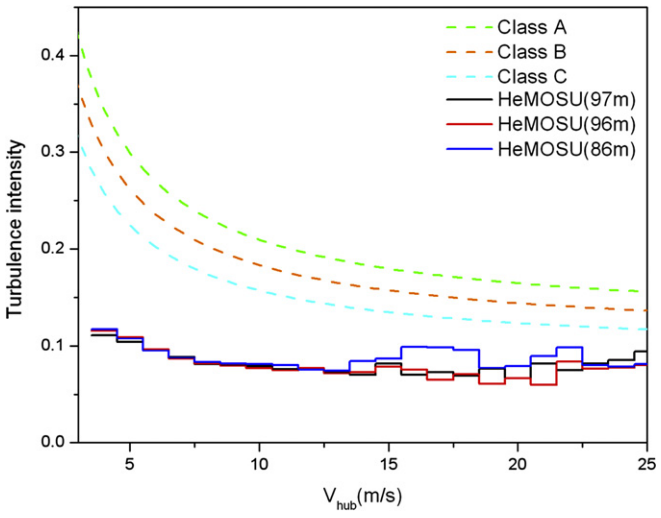

Fig. 10. Turbulence intensity.

Table 6
Estimation of AEP and C.F. (c: 7.93, k: 1.8434).

Manufacturer	Turbine class	Rated power (kW)	Rotor diameter (m)	AEP (MWh)	AEP/MW (MWh)	C.F. (%)
Doosan	IA	3000	91.3	6850	2283	26.07
Doosan	IIA	3000	100	7291	2430	27.74
Gamesa	IIA	4500	128	13,450	2989	34.12
GE wind energy	IB	3600	104	8814	2448	27.95
Enercon	IA	7500	127	17,174	2290	26.14
REpower	IIA	3300	104	9141	2770	31.62
REpower	IB	5000	126	12,642	2528	28.86
Siemens	IA	3600	107	8985	2496	28.49
VESTAS	IA	2000	80	4835	2418	27.60
VESTAS	IIA	3000	90	6634	2211	25.24
VESTAS	IIA	3000	112	8983	2994	34.18

$$\mathrm{AEP} = \sum_{\mathrm{cut-in}}^{\mathrm{cut-out}} (P(v)\cdot f(v)\cdot 8760), \tag{7}$$

$$\mathrm{C.F.}(\%) = \frac{\mathrm{AEP}}{\text{Rated power} \times 8760} \times 100, \tag{8}$$

where $P(v)$ is the power curve of the wind turbine.

Mean wind speed was converted to that at the hub height of each wind turbine with the wind shear exponent. Mean wind speed is estimated by the long-term wind speed at 97 m height. The wind shear exponent is 0.13 calculated in Section 3.2. Because interest is focused only on the turbine's performance, the wake loss of the wind farm's layout has not been considered. Additional losses, such as availability of turbines and operational electrical efficiency, are assumed to be 10%.

In order for a turbine designed with a Turbine Class I to endure higher than the extreme load, it normally has shorter blades than a turbine designed with a Turbine Class II. Typically, the Capacity Factor of a Class II turbine is relatively lower than that of a Class I. Even though the recently developed VESTAS V112 has a rated output of 3 MW and its blades are 112 m in diameter, it has been certified as a class II turbine. The VESTAS V112, with the longest blades per unit of output, has the highest Capacity Factor. As the recently developed Repower 3300 has relatively long blades per unit of output, the Capacity Factor of the Repower 3300 is also higher than that of other turbines. The introduction of a wind turbine that has a high Capacity Factor as well as a high wind turbine class will catalyze the development of large-scale offshore wind farms.

5. Conclusion

This paper analyzed design parameters of a demo-farm such as mean wind speed, energy density, wind/energy rose, and air density using data measured from three metrological masts. In addition, wind turbine class is identified from extreme wind speed and turbulence intensity, and energy production is predicted with design basics. From this study, the following conclusions were obtained with respect to offshore demo-farms:

1. The wind energy potential of the demo-farm is Wind Class 3 in terms of energy density. The measured value is also similar to that shown on the KIER wind map as well as the long-term wind energy potential estimated by using MCP techniques. It can be concluded that the site selection is reasonable and the site of the demo-farm is suitable for the construction of offshore wind farms.
2. The wind rose shows that northwesters are predominant at the site. Since the major wind direction is distinct, a wind farm layout that takes into account the major wind direction will be the most efficient. In addition, meteorological characteristics such as typhoons and the monsoon should be taken into consideration.
3. The vertical wind profile shows that the wind shear exponent and the wind speed varied depending on the season. This difference is caused by monsoons and the frequency of typhoons in summer. Optimum O&M planning is scheduled utilizing this characteristic.
4. Measured air density is 2–4% higher than standard air density. It is expected that energy production at the demonstration wind farm will increase even when the same wind turbine is applied.
5. Through an analysis of extreme wind speed and turbulence intensity, we determined that Class II-C or higher wind turbines should be recommended for the site.
6. Analyses of AEP and C.F. show that the site of the demo-farm is economically feasible. The latest versions of wind turbines enhance the economic feasibility.

In the future, the design of demo-farms, turbines, and their foundations will be conducted using the estimated design basis of the abovementioned results.

Acknowledgements

This work was supported by the New & Renewable Energy of the Korea Institute of Energy Technology Evaluation and Planning (KETEP) grant funded by the Korea Government Ministry of Knowledge Economy (20113040020010).

References

[1] Rehman Sahfiqur, Ahmad Aftab. Assessment of wind energy potential for coastal locations of the Kingdom of Saudi Arabia. Energy 2004;29:1105–15.
[2] Onat Nevzat, Ersoz Sedat. Analysis of wind climate and wind energy potential of regions in Turkey. Energy 2011;36:148–56.
[3] Islam MR, Saidur R, Rahim NA. Assessment of wind energy potentiality at Kudat and Labuan, Malaysia using Weibull distribution function. Energy 2011; 36:985–92.
[4] Guo Zhenhai, Zhao Jing, Zhang Wenyu, Wang Jianzhou. A corrected hybrid approach for wind speed prediction in Hexi Corridor of China. Energy 2011; 36:1668–79.
[5] Carta José A, Velázquez Sergio. A new probabilistic method to estimate the long-term wind speed characteristics at a potential wind energy conversion site. Energy 2011;36:2671–85.
[6] Lim Hee-Chang, Jeong Tae-Yoon. Wind energy estimation of the Wol-Ryong coastal region. Energy 2010;35:4700–9.
[7] Ko Kyungnam, Kim Kyoungbo, Huh Jongchul. Variations of wind speed in time on Jeju Island, Korea. Energy 2010;35:3381–7.
[8] Jang Jea-Kyung, Yu Byoung-Min, Ryu Ki-Wahn, Lee Jun-Shin. Offshore wind resource assessment around Korean Peninsula by using QuikSCAT satellite data. Journal of the Korean Society for Aeronautical & Space Sciences 2009; 37(11):1121–30.
[9] Kim Hyun-Goo, Choi Jaeou, Lee Hwawoon, Jung Woosik. Study on the establishment of a wind map of the Korean Peninsula (I. Establishment of a synoptic wind map using remote-sensing data). Journal of the Korean Society for New and Renewable Energy 2005;1(1):1–10.
[10] Kim HG, Jang MS, Kyong NH, Lee HW, Choi HK, Kim DH. Establishment of the low- resolution national wind map by numerical wind simulation. Journal of the Korean Solar Energy Society 2006;26(4):31–8.
[11] Kim JY, Kang KS, Oh KY, Lee JS, Ryu MS. A study on the site selection of offshore wind farm around Korean Peninsula. In: Third international conference on ocean energy; 2009.
[12] Oh Ki-Yong, Kim Ji-Young, Lee Jun-Shin, Ryu Ki-Whan. Wind resource assessment around Korea Peninsula for feasibility study on 100 MW class offshore wind farm. Renewable Energy 2012;42:217–26.
[13] Oh Ki-Yong, Kim Ji-Young, Lee Jun-Shin. Assessment of wind resource around the Korean Peninsula by using marine buoys datasets. Journal of the Korean Society for New and Renewable Energy 2011;7(1):15–21.
[14] Jang Jea-Kyung, Ryu Ki-Wahn. Site-adaptive aerodynamic design of wind turbine and environmental impact assessment of its noise and electromagnetic interference, report no. R107715201. KEPRI – Ministry of Knowledge and Economics; Feb 2011.
[15] Woods JC, Watson SJ. A new matrix method of predicting long-term wind roses with MCP. Journal of Wind Engineering 1997;66:85–94.
[16] Oh Ki-Yong, Kim Ji-Young, Lee Jun-Shin. A study on the reduction of uncertainty in estimations of long term wind resources, using the complementary MCP (Measure-Correlate-Predict) technique. In: European wind energy conference; 2011.
[17] Frost W, Long B, Turner RE. Engineering handbook on the atmospheric environmental guidelines for use in wind turbine generator development. NASA technical paper 1359; 1978.
[18] Environmental conditions and environmental loads. DNV; 2007. DNV-RP-C205.
[19] Mortensen Niels G, Rathmann Ole, Nielsen Morten, Kelly Mark C, Gryning Sven-Erik, Troen Ib, et al. WAsP 10 course notes, Risø-I-2952 (8th ed.) (EN); 2011.
[20] IEC 61400 wind turbines – part 12-1: power performance measurements of electricity producing wind turbines. IEC; 2005.
[21] IEC 61400 wind turbines – part 1: design requirements. IEC; 2005.
[22] IEC 61400 wind turbines – part 3: design requirements for offshore wind turbines. IEC; 2008.
[23] Kotz S, Nadarajah S. Extreme value distributions. Theory and applications. London: Imperial College, Press; 2000.